HHS Public Access

Author manuscript

*J Am Chem Soc*. Author manuscript; available in PMC 2024 July 19.

Published in final edited form as:

*J Am Chem Soc*. 2023 July 19; 145(28): 15197–15206. doi:10.1021/jacs.3c02033.

# Design of tetrazolium cations for the release of antiproliferative formazan chelators in mammalian cells

**Zoufeng Xu**[1,‡], **Yu-Shien Sung**[1,‡], **Elisa Tomat**[1]

[1]Department of Chemistry and Biochemistry, The University of Arizona, 1306 E. University Blvd., Tucson AZ 85721 (USA)

## Abstract

Cancer cells generally present a higher demand for iron, which plays crucial roles in tumor progression and metastasis. This iron addiction provides opportunities to develop broad-spectrum anticancer drugs targeting iron metabolism. In this context, prochelation approaches are investigated to release metal-binding compounds under specific conditions, thereby limiting off-target toxicity. Here, we demonstrate a prochelation strategy inspired by the bioreduction of tetrazolium cations widely employed to assess the viability of mammalian cells. We designed a series of tetrazolium-based compounds for the intracellular release of metal-binding formazan ligands. The combination of reduction potentials appropriate for intracellular reduction and an *N*-pyridyl donor on the formazan scaffold led to two effective prochelators. The reduced formazans bind as tridentate ligands and stabilize low-spin Fe(II) centers in complexes of 2:1 ligand-to-metal stoichiometry. The tetrazolium salts are stable in serum for over 24 h, and antiproliferative activities at micromolar levels were recorded in a panel of cancer cell lines. Additional assays confirmed the intracellular activation of the prochelators and their ability to affect cell cycle progression, induce apoptotic death, and interfere with iron availability. Demonstrating the role of iron in their intracellular effects, the prochelators impacted the expression levels of key iron regulators (i.e., transferrin receptor 1, ferritin), and iron supplementation mitigated their cytotoxicity. Overall, this work introduces the tetrazolium core as a platform to build prochelators that can be tuned for activation in the reducing environment of cancer cells and produce antiproliferative formazan chelators that interfere with cellular iron homeostasis.

## Graphical Abstract

Corresponding Author Elisa Tomat – Department of Chemistry and Biochemistry, The University of Arizona, Tucson AZ 85721-0041. tomat@arizona.edu.

‡Author Contributions

These authors contributed equally. The manuscript was written through contributions of all authors. All authors have given approval to the final version of the manuscript.

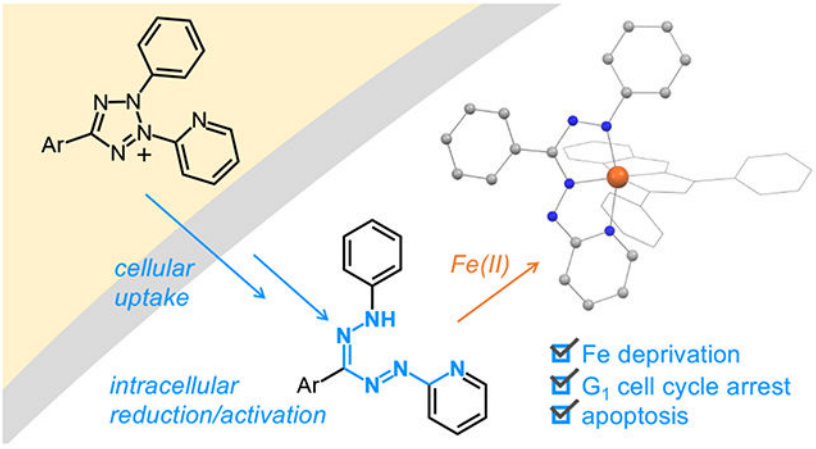


**Keywords**

Tetrazolium; Formazan; Bioreductive activation; Iron; Prochelator; Cancer

## Introduction

An altered iron metabolism and homeostasis characterizes cancer cells, which exhibit an increased dependence on iron when compared to normal cells.[1, 2] For instance, malignant cells increase iron import through the overexpressed transferrin receptor and limit iron release by degrading exporter ferroportin.[3] In addition, iron is implicated in the crosstalk between neoplastic cells and macrophages,[4] cancer stem cells,[5] and other components of the tumor microenvironment that promote growth, metastasis, and resistance to therapy.[6] Overall, the role of iron in cancer biology is being recognized for its potential prognostic value[7] and therapeutic relevance.[8, 9] The polypharmacological nature of iron-targeting approaches, which inherently affect multiple cellular processes, is an advantage in efforts to overcome resistance in single-drug interventions or in combination with other anticancer drugs.[10, 11]

Iron-sequestering agents that are employed clinically to treat iron overload,[12] such as FDA-approved chelators deferoxamine (DFO) and deferasirox (DFX, Fig. 1a), were tested in early clinical trials for cancer indications.[13] More recent clinical studies have included tridentate thiosemicarbazones (triapine, DpC, Fig. 1a), which have mechanisms of action that involve both iron binding and intracellular redox chemistry.[14, 15] Although iron chelating agents have shown promising results in clinical trials, and some such studies are still ongoing, to date no iron chelator has been approved for cancer chemotherapy.

Multiple current efforts on the development of metal-binding pharmaceuticals involve prochelation approaches, in which a metal donor group is typically masked for release under specific conditions (Fig. 1b). Prochelation strategies serve to improve membrane permeability and/or selectivity of a chelator while avoiding off-target effects due to indiscriminate metal sequestration.[16-18] For instance, the phenolate donor of DFX and its derivatives has been masked with boronate-containing groups (that are activated

by hydrogen peroxide)[19] or phosphate esters (to be unmasked by phosphatases).[20] Alternatively, several prochelators have been designed for activation by specific enzymes, such as γ-glutamyl transferase[21] or β-glucosidase.[22]

For anticancer applications, reductive activation strategies capitalize on the reducing intracellular environment that characterizes malignant cells.[23, 24] Reactivity in the presence of high glutathione (GSH) concentrations intracellularly (i.e., 1-10 mM) has been employed to release masked anticancer agents, including ionophores and chelators.[16] We have developed a prochelation strategy based on the use of disulfide or sulfonate groups to mask the tridentate binding unit of thiosemicarbazone (e.g., $(TC1\text{-}S)_2$, Fig. 1c) and aroylhydrazone chelators.[25-29] Upon cellular uptake, the reduction of the disulfide bond releases a tridentate thiolate chelator that coordinates iron in mammalian cells. The disulfide linkage can also be employed to connect a biomolecule, such as a monosaccharide[30, 31] or albumin,[32] to improve the cancer selectivity of the constructs and enhance their therapeutic window.

Herein, we demonstrate a reductive prochelation approach based on the intracellular reduction of tetrazolium ions resulting in metal-binding formazans. We introduce a family of prochelators inspired by the well-known reagent 5-(4,5-dimethylthiazol-2-yl)-1,3-diphenyltetrazolium bromide (MTT, Fig. 2a), which is widely used to assess proliferation and viability in mammalian cell culture (i.e., MTT assay).[33, 34] The intracellular reduction of the tetrazolium cation MTT, which is primarily attributed to oxidoreductase enzymes,[35] leads to formazan MTF (Fig. 2a).[33] The associated color change from yellow to purple is detected colorimetrically in several histology and bioimaging applications.[33]

Based on this well-established reactivity, we reasoned that the tetrazolium motif could serve as an attractive platform for reductively activatable prochelators. Rather than masking one metal donor group on the chelator structure, this approach ‘wraps’ the metal-binding unit into the cationic tetrazolium core (Fig. 2b). Intracellular reduction is then expected to release a formazan compound, namely a member of a well-known class of ligands for metal coordination.[36] Tetrazolium compounds offer two key advantages as potential prochelators: (i) their amphiphilic nature makes them soluble in aqueous solutions and also capable of rapidly permeating cell membranes;[33] and (ii) their reactivity/activation can likely be tuned via synthetic modification of the ring substituents. Although the parent compound MTT is prone to react with bioreductants (e.g., ascorbate, GSH) in blood serum,[37, 38] we anticipated that alterations of the tetrazolium structure could also serve to increase stability in a variety of biological settings.

## Results and Discussion

### Synthesis and Properties of Formazan Chelators

The coordination chemistry of formazanate complexes has showcased the versatility of the NNCNN backbone, which can bind metal cations through different coordination modes.[36] Asymmetric formazan ligands featuring a metal-binding *N*-aryl group, such as the thiazole ring in MTF, typically bind as tridentate ligands with five-membered formazanate chelates (*vide infra*).[39] To prepare a prototypic series of formazan chelators, we first sought to

replace the dimethylthiazole ring with alternative iron-binding moieties (Fig. 3), thus maintaining a tridentate coordination common to several effective iron chelators (e.g., DFX, Triapine, DpC, Fig. 1a).

The structures of the formazan compounds investigated in this study are shown in Fig. 3 in the 'closed' *s-cis* conformation. Compound **1a**, featuring a benzothiazole ring as $Ar^5$, was chosen because Fe(II) coordination of this formazan ligand has been reported.[39] We then introduced pyridyl (**2a**) and 2-hydroxyphenyl (**3a**) rings at the $Ar^5$ position because these known iron-binding donors are found in multiple chelators (e.g., DFX, Triapine, DpC, Fig. 1a). In structures **4a** and **5a**, we also added pyridyl and 2-hydroxyphenyl rings at the $Ar^3$ position. Lastly, **6a** and **7a** maintain the pyridyl and 2-hydroxyphenyl donors in $Ar^3$, respectively, but lack metal-binding donors at *N*-$Ar^5$, which is occupied by a phenyl ring.

MTF was obtained in high yield from the reduction of commercially available MTT with ascorbic acid (see ESI for experimental details). Conversely, the planned cohort of formazan compounds **1a**–**7a** was prepared via the well-established reaction of diazonium salts and hydrazone precursors in basic conditions in DMF (Scheme S1 and Table S1).[36, 40] In all cases, the desired diazonium salt was obtained from treatment of an aromatic amine with sodium nitrite in acidic aqueous solution at low temperature and used directly in next step (Scheme S1 and Table S1).

The iron-binding ability of the formazan compounds was tested in aqueous mixtures (50 mM HEPES and DMSO, 7:3, v/v, pH 7.4) in the presence of Fe(II) (1.0 equiv.). The solutions of compounds **2a** and **4a** exhibited a marked color change from yellow/orange to red/violet upon iron addition, whereas the changes were less pronounced in other cases and absent for **6a** and **7a** (Fig. S1). For compounds **1a**–**5a** the reaction was complete within 16 min, and **4a** clearly exhibited the fastest binding kinetics with full complexation within 4 min. High-resolution mass spectrometry (Table S2) corroborated the formation of iron complexes of 2:1 ligand-to-metal stoichiometry in the case of MTF and formazans **1a**–**5a** under these conditions. In contrast, complexes of **6a** and **7a** were not detected by mass spectrometry. HPLC-HRMS analysis of the reaction mixtures did not detect any iron coordination of **6a** and **7a**, whereas the 2:1 complexes were the only products observed for **2a** and **4a** (Fig. S2). Collectively, these findings in aqueous solutions indicated that a coordinating *N*-aryl group (i.e., thiazole, pyridyl, hydroxyphenyl) is required for iron binding and that the *N*-pyridyl analogs, particularly **4a**, are the most promising chelators in this cohort.

The relative Fe(II) binding efficacy of formazans **2a** and **4a** was assessed *in vitro* using calcein,[41] a fluorescent probe that is commonly employed to monitor changes in the cytosolic labile iron pool (*vide infra*).[42] Calcein is mostly quenched when bound to Fe(II) (1.0 equiv, $K_d$ = 0.14 μM),[42] but fluorescence is restored when chelators displace iron from the probe. In our aqueous mixture (50 mM HEPES buffer at pH 7.4 and MeOH, 3:1 v/v), DFX outcompetes calcein to fully restore its initial fluorescence, whereas formazans **2a** and **4a** result in partial restoration (Fig. S3). In contrast, **6a** and citric acid, which is a common ligand of biological iron,[43] fail to displace calcein-bound iron(II). Overall, these data show

that **2a** and **4a** compete successfully with calcein for iron coordination, but their affinity is lower than that of iron scavenger DFX.[44]

As expected for ligands featuring an “all-nitrogen” binding unit, formazans **2a** and **4a** do not coordinate oxophilic cations Ca(II) and Mg(II) (Fig. S4), which are abundant in biological settings. Conversely, both chelators bind late transition metals Cu(II) and Zn(II), in line with the known coordination chemistry of formazans.[36] With picomolar (or lower) intracellular concentrations,[45] however, these ions do not impact the overall binding of micromolar iron by chelators in the cytosol.[46]

## Iron Complexes of Formazan Chelators

Having confirmed the formation of 2:1 complexes in solution, we sought to characterize the binding mode of *N*-pyridyl formazans **2a** and **4a**. In addition, we isolated the iron complex of **MTF** because this hypothesized species inspired this study but has not been characterized crystallographically.

Addition of $Fe(BF_4)_2{\cdot}6H_2O$ (1.0 equiv.) to solutions of the formazan ligands in THF at room temperature led to Fe(II) complexes of 2:1 ligand-to-metal stoichiometry (Fig. 4) as confirmed by high-resolution mass spectrometry and elemental analysis. NMR data indicated that the two ligands coordinate in the same way and that the complexes are diamagnetic, therefore Fe(II) presents a low-spin electronic configuration in all three species (see ESI for details).

Single-crystal diffraction analysis revealed distorted octahedral complexes with two monoanionic tridentate ligands (Fig. 4, Table S3). The absence of counterions confirms the ferrous oxidation state for the iron center. The aromatic nitrogen donor (i.e., thiazole in **MTF** and pyridine in **2a** and **4a**) forms a five-membered chelate involving the N3 atom of the formazanate backbone. A second, adjacent five-membered chelate is provided by the deprotonated formazanate moiety binding through the N1 donor. This coordination mode was previously reported for **1a** and other asymmetric formazan ligands featuring a metal-binding *N*-aryl group.[39, 47] The presence of the hydroxyphenyl $Ar^3$ substituent in formazan **4a** does not result in a different coordination mode: instead, in Fe(**4a**–*H*)$_2$ the hydroxyl group is engaged in a hydrogen-bonding interaction with N4 on the formazan scaffold.

The observed Fe–N distances for the formazanate donors (i.e., N1 and N3) range from 1.864(2) to 1.946(3) Å, similar to those in other low-spin Fe(II) complexes with tridentate formazanates (Table S4).[39, 47, 48] In all three complexes, the bonds to the heteroaryl N donors are slightly longer (up to 2.009(4) Å in Fe(MTF–*H*)$_2$). The N–N and N–C distances along the formazanate backbone (i.e., N1-N2-C7-N3-N4) range narrowly between 1.311(4) and 1.371(4)) Å and are consistent with charge delocalization on the conjugated anionic ligand.

The isolated complexes are stable with respect to oxidation under aerobic conditions: the formazan ligands **MTF**, **2a** and **4a**, with a (*N*, *N*, *N*) donor set, stabilize the iron center in the ferrous oxidation state. As observed for tridentate thiosemicarbazone chelators, the

presence of rather soft nitrogen donors favors Fe(II) complexes whereas harder oxygen donors typically lead to Fe(III) species.[14] The cyclic voltammograms of the three complexes (recorded in DMF, Fig. S5) exhibit a reversible one-electron oxidation at potentials similar to that of the ferrocene reference ($Fc^+/Fc$, $E_{1/2}$ 0.70 V vs NHE).[49] In fact, coordination studies with similar formazan ligands reported the formation of Fe(II) complexes even in the presence of a Fe(III) source (i.e., $FeCl_3$) and hypothesized the oxidation of a portion of the ligand (i.e., forming the tetrazolium cation) to produce the coordinating Fe(II).[39, 47] Because the intracellular labile iron pool consists largely of ferrous species, this type of reactivity is not a concern for our intended application.

## Synthesis and Properties of Tetrazolium Prochelators

The tetrazolium compounds (Fig. 3) were synthesized from the formazans by oxidation with *N*-bromosuccinimide (NBS) (Scheme S2, and Table S5). For structures featuring a 2-hydroxyphenyl group, the oxidation was carried out on methoxyphenyl precursors (**3a-OMe**, **4a-OMe**, **5a-OMe**, **7a-OMe**, Scheme S2) to avoid unwanted oxidative reactivity at the phenolic position. A demethylation step in the presence of $BBr_3$ then afforded **3b**, **4b**, **5b**, and **7b** (Scheme S2 and Table S5). All the tetrazolium compounds were isolated as bromide salts.

As expected for compounds featuring a positively charged tetrazolium core, no indication of iron binding was observed in buffered aqueous solutions in the presence of Fe(II) (Fig. S6). Given the ability of formazans **1a**–**5a** to coordinate Fe(II) in aqueous media, tetrazolium cations **1b**–**5b** could therefore serve as prochelators if reductively activated in cells.

The distribution coefficients (log $D_{o/pH7.4}$, Table 1) of the tetrazolium compounds were determined experimentally to assess their lipophilicity at biologically relevant pH. The obtained values were generally close to zero, consistent with the amphiphilicity of the triaryltetrazolium scaffold.[33] In this small cohort of rather similar cations, the hydroxyphenyl group rendered compounds more hydrophobic whereas the pyridyl group shifted values towards more negative hydrophilic values; however, all compounds were found to be well distributed between the organic and aqueous phases.

The reduction potentials ($E_{red}$) of all the tetrazolium salts were investigated by cyclic voltammetry in phosphate buffered saline solution (PBS, pH 7.4) using potassium ferricyanide as a reference ($K_3FeCN_6$, $E_0$ 0.430 V vs NHE).[50] These salts present excellent solubility in aqueous media and 2 mM solutions were prepared for electrochemical testing. For each compound, the voltammogram shows an irreversible two-electron reduction at a potential that varies considerably depending on the identity of the aryl substituents on the tetrazolium core. As reported previously for aqueous tetrazolium solutions,[51] the peaks are rather broad and encompass two one-electron reduction events as well the protonation of the resulting formazanate. Furthermore the disproportionation of the tetrazolinyl radical is a known component of tetrazolium reductions.[52] In general, the recorded potentials (Table 1, Fig. S7) indicate that the reduction of tetrazolium cations can be easily tuned through synthetic modification and hence serve as an advantageous characteristic for the development of reductive prochelation strategies. As expected, electron-withdrawing *N*-Ar groups (e.g., thiazolyl, benzothiazolyl, pyridyl) shift the reduction anodically to more

positive potentials. The reduction of prochelators **2b** and **4b**, leading to the most promising chelators **2a** and **4a**, was also reproduced chemically in the presence of naturally occurring reductant ascorbate at pH 7.4 (Fig. S7).

The intracellular reduction of MTT occurs in multiple compartments, including the cytoplasm and mitochondria, and relies primarily on NADPH-dependent oxidoreductase enzymes; however, the involvement of other redox enzymes, different electron donors, and non-enzymatic reactivity is also possible.[35] In this context, the recorded peak potentials of our tetrazolium compounds (Table 1, Fig. S7) were taken as simple indicators of their relative thermodynamic tendency to be reduced under similar conditions. MTT and benzothiazole analog **1b** are reduced at easily accessible potentials. Conversely, the thermodynamically stable compounds **3b** ($E_p$ = −328 mV) and **5b** ($E_p$ = −380 mV) are significantly harder to reduce and, in the middle of our observed range, the reduction potentials of compounds **2b**, **4b**, **6b** and **7b** make them potentially well suited for release of the corresponding formazans in the intracellular environment.

The reduction kinetics of the tetrazolium cations were investigated by HPLC analysis in fetal bovine serum (FBS) (Table 1 and Fig. S8), which contains several biological reductants and is relevant to the utilization of these compounds as prochelators in mammalian cells. Benzothiazole analog **1b** ($E_p$ = 207 mV) undergoes the fastest reduction and has a half-life ($t_{1/2}$) of 2 h, with only 2% remaining after 24 h. Thiazole-based MTT ($E_p$ = 94 mV) is also reduced in serum, but its $t_{1/2}$ is longer than 24 h and 58% remained after 24 h. The chromatograms (Fig. S50) confirm their reduction (producing **1a** and MTF, respectively) in FBS as previously reported.[37, 38] All the tetrazolium compounds with intermediate (**2b**, **4b**, **6b** and **7b**) or lower (**3b** and **5b**) reduction potentials in our series do not undergo reduction in FBS. These results are consistent with the electrochemically measured reduction potentials and indicate that compounds **2b**-**7b** are stable in the extracellular milieu.

## Antiproliferative Activity of Tetrazolium Prochelators

For our first tests of antiproliferative activities, we chose a panel of cancer cell lines of different origin (ovarian A2780, breast MDA-MB-231, colon Caco-2, and lung A549) because the importance of iron in cancer progression is well established in these cancer types.[53-55] As a comparison, normal lung fibroblasts (MRC-5) were included in the panel. The optical absorption of all the activated formazans falls broadly in the visible range (400–800 nm) overlapping with that of many colorimetric probes for viability assays. Therefore, we employed the emission-based resazurin assay, which monitors the reduction of the probe to brightly fluorescent resorufin. The $IC_{50}$ values after 72-hour incubations are shown in Table 1.

DFX was employed as a control compound known to display antiproliferative activity due to iron deprivation.[56] In addition, its structure, which features multiple aromatic rings, a triazole core, and phenolic metal-binding donors (Fig. 1a), is in part related to those of the tetrazolium and formazan compounds we are investigating. In general agreement with previous reports in various cell lines,[57, 58] the $IC_{50}$ values for DFX were in the (15–67 μM) range in the cancer cells and up to 220 μM in the normal fibroblasts, which are typically less susceptible to iron deprivation.

MTT and **1b**, which have limited stability in serum, present moderate antiproliferative activities in the tested cancer cells. Conversely, compounds **6b** and **7b**, which do not bind iron in aqueous solutions, show low activity throughout this cell panel. Compounds **3b** and **5b**, which have the lowest reduction potentials, are also rather inactive in the tested cell lines (with most $IC_{50}$ values above 200 μM).

Among the tetrazolium salts in our series, **2b** and **4b** present the most promising antiproliferative activities, with $IC_{50}$ values ranging from 12 to 30 μM in the tested cancer cell lines and above 160 μM in normal cells. These amphiphilic compounds are reduced at accessible potentials, and the corresponding formazans promptly coordinate Fe(II). Interestingly, in spite of their limited solubility in aqueous solutions, formazans **2a** and **4a** are antiproliferative at submicromolar levels in the tested cancer cells and below 30 μM in normal cells (Table S6). These lipophilic compounds, which do not require intracellular activation, possibly attain effective cellular uptake and iron sequestration. Extracellular metal binding and ionophore activity may also be involved. Although the mechanism of toxicity of formazans remains to be determined, the reduction of tetrazolium prochelators provides an effective strategy to deliver antiproliferative compounds to the intracellular environment. Optimization of the activation step is likely to produce prochelators of higher therapeutic indexes.

## Effects on cell cycle, cell death and intracellular iron

The antiproliferative effects of iron chelators are often associated with cell cycle arrest and promotion of apoptosis.[13] Because iron depletion affects multiple cell cycle regulators, including cyclins, cyclin-dependent kinases, and p53, the impact of chelators on cell cycle progression is complex but typically results in $G_1$ or S arrest.[59]. For instance, DFX was found to elicit $G_1$ or S arrest depending on cell line[60] or concentration.[61] In A2780 cells, we found that our lead tetrazolium compounds **2b** and **4b** elicited a significant increase in the cell population in the $G_1$ phase after 24-h incubations (Figs. 5a, S9). In the same conditions, incubation with DFX caused S-phase arrest.

In tests of apoptosis following 48-h incubations, we observed a slight increase in the fraction of cells undergoing early apoptosis and a large increase of cells at the late apoptotic stage (Figs. 5b, S10). This effect was more prominent for **4b** (i.e., 30% of cells in late apoptosis) compared to **2b** (15%) and lower than that in the control DFX (42%).

Having confirmed cell cycle arrest at the $G_1$ phase and induction of apoptosis, we sought to investigate more directly the ability of **2b** and **4b** to interfere with intracellular iron availability. In these experiments, besides the positive control DFX, the tetrazolium salt **6b** was added as a negative control. This compound has a comparable reduction potential to **2b** and **4b**; however, its reduction product **6a** does not bind Fe(II) in aqueous solutions (Figs. S1-S2 Table S2).

Changes of the cytosolic labile iron pool were monitored through the calcein assay, which detected iron coordination by **2a** and **4a** *in vitro* (Fig. S3). We used the acetoxymethyl precursor (calcein-AM) to deliver calcein to the cytosol, where it is partially quenched by paramagnetic iron ions.[62] After 24-h incubations in A2780 cells, DFX and prochelators

**2b** and **4b** liberate a fraction of iron-bound calcein and increase fluorescence by ~54%, ~37% and ~68%, respectively (Fig. 6a). In contrast, negative control **6b** did not elicit a fluorescence change. The emission increased with longer incubation times (i.e., 1h, 3h, and 24h) for DFX and **2b**, but was saturated within 1 h when incubating with **4b**. This observation suggests a faster cellular uptake and/or activation of this cationic species, which has a higher distribution coefficient and more accessible reduction potential relative to the **2b** analog (Table 1). In MRC-5 cells, only DFX led to increased fluorescence (by ~34% at 24 h, Fig. 6b) whereas prochelators **2b** and **4b** did not show evidence of iron binding in the same conditions, likely indicating a lower extent of activation in the normal fibroblasts.

To confirm directly the formation of the complexes in A2780 cells, we analyzed cell lysates through uHPLC-HRMS: following 48-h incubations with prochelators **2b** and **4b** (40 μM), the intact tetrazolium compounds were detected along with formazans **2a** and **4a** and the corresponding iron complexes of 2:1 ligand-to-metal stoichiometry (Fig. S11). Although the detection of the intact prochelators indicates only partial activation, we sought to determine the effects of the produced formazans on intracellular iron availability.

Probing the ability of tetrazolium prochelators **2b** and **4b** to impact iron signaling, we investigated the expression levels of two critical handlers of biological iron: transferrin receptor 1 (TfR1) and ferritin (Fig. 7). TfR1 is the transmembrane protein responsible for the uptake of iron-import protein transferrin, whereas ferritin is the primary iron-storage protein in the cytosol. We assessed by Western blot analysis the expression of TfR1 and of ferritin heavy chain (i.e., ferritin H), one of the subunits of the globular ferritin complex. Both proteins are post-transcriptionally regulated by iron regulatory proteins (IRPs), and it is well established that intracellular iron deficiency causes an increase of TfR1 expression concurrent with the degradation of ferritin.[63] This effect was confirmed upon incubation with iron chelator DFX; conversely, iron supplementation of the growth media with ferric ammonium citrate (FAC) caused a decrease of TfR1 and an increase of ferritin H levels as expected in the presence of abundant iron. In the same incubation conditions (40 μM, 24 h), **2b** and **4b** led to increased TfR1 expression but decreased ferritin H levels in A2780 cancer cells, consistent with a perturbation of intracellular iron availability (Fig. 7a). In normal MRC-5 cells, however, the effects were weaker: **4b** had an impact only on ferritin H, whereas **2b** did not affect significantly either expression level (Fig. 7b). Notably, both controls DFX and FAC maintained similar effects, albeit less pronounced within the generally lower expression levels of both TfR1 and ferritin H in the normal fibroblasts. Lastly, tetrazolium **6b** did not significantly alter the expression of iron handlers when compared to the untreated control in both cancer and normal cells.

Overall, the effects of compounds **2b** and **4b** on intracellular iron in A2780 cancer cells (Figs. 6a and 7a) are consistent with a prochelation mechanism involving (i) reduction/activation of the tetrazolium species and (ii) iron sequestration by the resulting formazan chelators. In addition, the intracellular calcein assays and immunoblotting experiments indicated that the tetrazolium prochelators are less potent in normal cells (Figs. 6b and 7b), consistent with less effective activation in the less reducing environment of normal fibroblasts.

We then examined the role of iron availability in the cytotoxicity of the tetrazolium prochelators **2b** and **4b**. Specifically, we employed fixable viability dyes (i.e., LIVE/DEAD kit) to determine the fraction of dead cells by flow cytometry after treatment with the test compounds (40 μM, 48 h) in the presence or absence of iron supplementation. We found that A2780 cells exposed to DFX, **2b** and **4b** could be rescued by iron supplementation through co-incubation with FAC (50 μM) or human holo-transferrin (holo-Tf, 50 μM) (Figs. 8 and S12). For instance, the percentage of dead cells after incubation with **4b** went from 12% to 2.4% or 6.2% in the presence of FAC or holo-Tf, respectively. The effect was more pronounced for DFX, possibly reflecting the fact that this chelator can be inactivated by iron binding before cellular uptake whereas the tetrazolium prochelators require intracellular reduction prior to iron binding. Even so, an increase of intracellular iron levels was found to decrease significantly the percentage of dead cells upon treatment with **2a** and **4b**. In contrast, the negative control **6b** did not present cytotoxicity and no changes were observed upon iron supplementation. Collectively, these iron-rescue experiments indicate that the cytotoxicity of tetrazolium compounds **2b** and **4b** is associated at least in part to iron deprivation and is therefore consistent with the prochelation design strategy.

## Conclusions

We have designed a prochelation strategy inspired by the intracellular reduction of tetrazolium ions in cellular viability assays. The approach takes advantage of the cellular uptake of triaryltetrazolium cations and their intracellular reduction to release formazan species, which are well-established ligands for transition metals. Unlike DFX and other conventional chelators, the cationic tetrazolium compounds are unable to bind metals prior to intracellular activation and are therefore poised to avoid systemic metal chelation and related off-target effects in therapeutic applications.

Through the synthesis and characterization of a series of tetrazolium and formazan compounds, we identified two tetrazolium-based prochelators (i.e., **2b** and **4b**) featuring a metal-binding *N*-pyridyl group. The corresponding formazan compounds behave as tridentate monoanionic ligands in the formation of low-spin Fe(II) complexes of 2:1 ligand-to-metal stoichiometry. Prochelators **2b** and **4b** are stable in serum, but susceptible to intracellular reduction. Their antiproliferative activities are in the micromolar range (i.e., $IC_{50}$ 12-30 μM, 72 h) in a panel of four cancer cell lines, whereas non-malignant fibroblasts are significantly less affected in the same conditions (i.e., $IC_{50}$ >160 μM, 72 h). In A2780 ovarian carcinoma cells, we found that **2b** and **4b** alter cell cycle progression, induce apoptosis, and interfere with iron availability, thereby impacting the expression of key iron handlers (i.e., TfR1 and ferritin). Consistent with antiproliferative activities due (at least in part) to iron deprivation, cells exposed to these prochelators are rescued by iron supplementation.

In summary, we have demonstrated a new prochelation approach that relies on the reductive activation of tetrazolium cations to form metal-binding formazan species upon cellular uptake. Because of the optical absorption of formazans in the near-infrared region (600-800 nm), this prochelation approach could be combined with metal sensing via photoacoustic methods in biological settings.[64] This new class of prochelators could be employed in

a variety of drug discovery and/or bioimaging efforts targeting the multifaceted role of transition metals in human health.

## Supplementary Material

Refer to Web version on PubMed Central for supplementary material.

## ACKNOWLEDGMENTS

We thank Dr. Andrei V. Astashkin and Iva Habensus for assistance with X-ray data acquisition and analysis. We also thank Aunita Hakimi for assistance with the Western blot experiments.

### Funding Sources

This work was supported by the US National Institutes of Health (R01 GM127646). The Bruker NEO-500 spectrometer in the UArizona Dept. of Chemistry and Biochemistry NMR Facility was purchased thanks to support from the National Science Foundation (MRI award CHE-1920234). The UArizona Cancer Center Flow Cytometry Shared Resource is supported by the National Cancer Institute (award P30 CA023074).

## REFERENCES

1. Richardson DR; Kalinowski DS; Lau S; Jansson PJ; Lovejoy DB Cancer cell iron metabolism and the development of potent iron chelators as anti-tumour agents. Biochim. Biophys. Acta 2009, 1790, 702–717. [PubMed: 18485918]
2. Torti SV; Torti FM Iron and cancer: more ore to be mined. Nat. Rev. Cancer 2013, 13, 342–355. [PubMed: 23594855]
3. Guo Q; Li L; Hou S; Yuan Z; Li C; Zhang W; Zheng L; Li X The role of iron in cancer progression. Front. Oncol 2021, 11, 778492. [PubMed: 34858857]
4. DeRosa A; Leftin A The Iron Curtain: Macrophages at the Interface of Systemic and Microenvironmental Iron Metabolism and Immune Response in Cancer. Front. Immunol 2021, 12, 614294. [PubMed: 33986740]
5. Recalcati S; Gammella E; Cairo G Dysregulation of iron metabolism in cancer stem cells. Free Radic. Biol. Med 2019, 133, 216–220. [PubMed: 30040994]
6. Jung M; Mertens C; Tomat E; Brüne B Iron as a Central Player and Promising Target in Cancer Progression. Int. J. Mol. Sci 2019, 20, 273. [PubMed: 30641920]
7. Miller LD; Coffman LG; Chou JW; Black MA; Bergh J; D'Agostino R Jr.; Torti SV; Torti FM An iron regulatory gene signature predicts outcome in breast cancer. Cancer Res. 2011, 71, 6728–6737. [PubMed: 21875943]
8. Tomat E Targeting iron to contrast cancer progression. Curr. Opin. Chem. Biol 2023, 74, 102315. [PubMed: 37187095]
9. Abbasi U; Abbina S; Gill A; Takuechi LE; Kizhakkedathu JN Role of iron in the molecular pathogenesis of diseases and therapeutic opportunities. ACS Chem. Biol 2021, 16, 945–972. [PubMed: 34102834]
10. Ninomiya T; Ohara T; Noma K; Katsura Y; Katsube R; Kashima H; Kato T; Tomono Y; Tazawa H; Kagawa S; Shirakawa Y; Kimura F; Chen L; Kasai T; Seno M; Matsukawa A; Fujiwara T Iron depletion is a novel therapeutic strategy to target cancer stem cells. Oncotarget 2017, 8, 98405–98416. [PubMed: 29228699]
11. Jansson PJ; Kalinowski DS; Lane DJR; Kovacevic Z; Seebacher NA; Fouani L; Sahni S; Merlot AM; Richardson DR The renaissance of polypharmacology in the development of anti-cancer therapeutics: Inhibition of the “Triad of Death” in cancer by Di-2-pyridylketone thiosemicarbazones. Pharmacol. Res 2015, 100, 255–260. [PubMed: 26318762]
12. Liu ZD; Hider RC Design of iron chelators with therapeutic application. Coord. Chem. Rev 2002, 232, 151–171.

13. Kalinowski DS; Richardson DR The evolution of iron chelators for the treatment of iron overload disease and cancer. Pharmacol. Rev 2005, 57, 547–583. [PubMed: 16382108]
14. Heffeter P; Pape VFS; Enyedy ÉA; Keppler BK; Szakacs G; Kowol CR Anticancer Thiosemicarbazones: Chemical Properties, Interaction with Iron Metabolism, and Resistance Development. Antioxid. Redox Signal. 2019, 30, 1062–1082. [PubMed: 29334758]
15. Merlot MA; Kalinowski SD; Kovacevic Z; Jansson JP; Sahni S; Huang LHM; Lane JRD; Lok H; Richardson RD Exploiting Cancer Metal Metabolism using Anti-Cancer Metal-Binding Agents. Curr. Med. Chem 2019, 26, 302–322. [PubMed: 28685681]
16. Steinbrueck A; Sedgwick AC; Brewster JT; Yan K-C; Shang Y; Knoll DM; Vargas-Zúñiga GI; He X-P; Tian H; Sessler JL Transition metal chelators, pro-chelators, and ionophores as small molecule cancer chemotherapeutic agents. Chem. Soc. Rev 2020, 49, 3726–3747. [PubMed: 32525153]
17. Oliveri V; Vecchio G Prochelator strategies for site-selective activation of metal chelators. J. Inorg. Biochem 2016, 162, 31–43. [PubMed: 27297691]
18. Wang Q; Franz KJ Stimulus-Responsive Prochelators for Manipulating Cellular Metals. Acc. Chem. Res 2016, 49, 2468–2477. [PubMed: 27749047]
19. Kielar F; Wang Q; Boyle PD; Franz KJ A boronate prochelator built on a triazole framework for peroxide-triggered tridentate metal binding. Inorg. Chim. Acta 2012, 393, 294–303.
20. Sedgwick AC; Yan K-C; Mangel DN; Shang Y; Steinbrueck A; Han H-H; Brewster JT II; Hu X-L; Snelson DW; Lynch VM; Tian H; He X-P; Sessler JL Deferasirox (ExJade): An FDA-Approved AIEgen Platform with Unique Photophysical Properties. J. Am. Chem. Soc 2021, 143, 1278–1283. [PubMed: 33428381]
21. Bakthavatsalam S; Sleeper ML; Dharani A; George DJ; Zhang T; Franz KJ Leveraging γ-Glutamyl Transferase To Direct Cytotoxicity of Copper Dithiocarbamates against Prostate Cancer Cells. Angew. Chem. Int. Ed 2018, 57, 12780–12784.
22. Oliveri V; Viale M; Caron G; Aiello C; Gangemi R; Vecchio G Glycosylated copper(II) ionophores as prodrugs for β-glucosidase activation in targeted cancer therapy. Dalton Trans. 2013, 42, 2023–2034. [PubMed: 23174818]
23. Lee MH; Yang Z; Lim CW; Lee YH; Dongbang S; Kang C; Kim JS Disulfide-Cleavage-Triggered Chemosensors and Their Biological Applications. Chem. Rev 2013, 113, 5071–5109. [PubMed: 23577659]
24. Kennedy L; Sandhu JK; Harper ME; Cuperlovic-Culf M Role of Glutathione in Cancer: From Mechanisms to Therapies. Biomolecules 2020, 10, 1429. [PubMed: 33050144]
25. Chang TM; Tomat E Disulfide/thiol switches in thiosemicarbazone ligands for redox-directed iron chelation. Dalton Trans. 2013, 42, 7846–7849. [PubMed: 23591852]
26. Akam EA; Chang TM; Astashkin AV; Tomat E Intracellular reduction/activation of a disulfide switch in thiosemicarbazone iron chelators. Metallomics 2014, 6, 1905–1912. [PubMed: 25100578]
27. Akam EA; Utterback RD; Marcero JR; Dailey HA; Tomat E Disulfide-masked iron prochelators: effects on cell death, proliferation, and hemoglobin production. J. Inorg. Biochem 2018, 180, 186–193. [PubMed: 29324291]
28. Wu W; Sung Y-S; Tomat E Thiol-Reactive Arylsulfonate Masks for Phenolate Donors in Antiproliferative Iron Prochelators. Inorg. Chem 2022, 61, 19974–19982. [PubMed: 36455205]
29. Mertens C; Akam EA; Rehwald C; Brüne B; Tomat E; Jung M Intracellular Iron Chelation Modulates the Macrophage Iron Phenotype with Consequences on Tumor Progression. PLOS ONE 2016, 11, e0166164. [PubMed: 27806101]
30. Sung Y-S; Kerimoglu B; Ooi A; Tomat E Aroylhydrazone Glycoconjugate Prochelators Exploit Glucose Transporter 1 (GLUT1) to Target Iron in Cancer Cells. ACS Med. Chem. Lett 2022, 13, 1452–1458. [PubMed: 36105345]
31. Akam EA; Tomat E Targeting Iron in Colon Cancer via Glycoconjugation of Thiosemicarbazone Prochelators. Bioconjugate Chem. 2016, 27, 1807–1812.
32. Sung Y-S; Wu W; Ewbank MA; Utterback RD; Marty MT; Tomat E Albumin Conjugates of Thiosemicarbazone and Imidazole-2-thione Prochelators: Iron Coordination and Antiproliferative Activity. ChemMedChem 2021, 16, 2764–2768. [PubMed: 33974730]

33. Stockert JC; Horobin RW; Colombo LL; Blázquez-Castro A Tetrazolium salts and formazan products in cell biology: Viability assessment, fluorescence imaging, and labeling perspectives. Acta Histochem. 2018, 120, 159–167. [PubMed: 29496266]
34. van Meerloo J; Kaspers GJL; Cloos J Cell Sensitivity Assays: The MTT Assay. Methods Mol. Biol 2011, 731, 237–245. [PubMed: 21516412]
35. Berridge MV; Herst PM; Tan AS Tetrazolium dyes as tools in cell biology: New insights into their cellular reduction. Biotechnol. Annu. Rev 2005, 11, 127–152. [PubMed: 16216776]
36. Gilroy JB; Otten E Formazanate coordination compounds: synthesis, reactivity, and applications. Chem. Soc. Rev 2020, 49, 85–113. [PubMed: 31802081]
37. Funk D; Schrenk H-H; Frei E Serum albumin leads to false-positive results in the XTT and the MTT assay. BioTechniques 2007, 43, 178–186. [PubMed: 17824385]
38. Ghasemi M; Turnbull T; Sebastian S; Kempson I The MTT Assay: Utility, Limitations, Pitfalls, and Interpretation in Bulk and Single-Cell Analysis. Int. J. Mol. Sci. 2021, 22, 12827. [PubMed: 34884632]
39. Brown DA; Bögge H; Lipunova GN; Müller A; Plass W; Walsh KG Iron and manganese complexes of benzothiazolyformazans. Inorg. Chim. Acta 1998, 280, 30–38.
40. Nineham AW The Chemistry of Formazans and Tetrazolium Salts. Chem. Rev 1955, 55, 355–483.
41. Wang Q; Franz KJ Modifying aroylhydrazone prochelators for hydrolytic stability and improved cytoprotection against oxidative stress. Bioorg. Med. Chem. 2018, 26, 5962–5972. [PubMed: 30429096]
42. Epsztejn S; Kakhlon O; Glickstein H; Breuer W; Cabantchik ZI Fluorescence Analysis of the Labile Iron Pool of Mammalian Cells. Anal. Biochem 1997, 248, 31–40. [PubMed: 9177722]
43. Königsberger L-C; Königsberger E; May PM; Hefter GT Complexation of iron(III) and iron(II) by citrate. Implications for iron speciation in blood plasma. J. Inorg. Biochem 2000, 78, 175–184. [PubMed: 10805173]
44. Steinhauser S; Heinz U; Bartholomä M; Weyhermüller T; Nick H; Hegetschweiler K Complex Formation of ICL670 and Related Ligands with $Fe^{III}$ and $Fe^{II}$. Eur. J. Inorg. Chem 2004, 2004, 4177–4192.
45. Ba LA; Doering M; Burkholz T; Jacob C Metal trafficking: from maintaining the metal homeostasis to future drug design. Metallomics 2009, 1, 292–311. [PubMed: 21305127]
46. Hider RC; Kong X Iron speciation in the cytosol: an overview. Dalton Trans. 2013, 42, 3220–3229. [PubMed: 23232973]
47. Gorbatenko YA; Rezinskikh ZG; Lipunova GN; Pervova IG; Maslakova TI; Slepukhin PA; Lipunov IN Synthesis and spectroscopic features of iron(II) 1-aryl-5-benzothiazol-2-ylformazanates. Russ. J. Appl. Chem 2008, 81, 2127–2131.
48. Milocco F; de Vries F; Siebe HS; Engbers S; Demeshko S; Meyer F; Otten E Widening the Window of Spin-Crossover Temperatures in Bis(formazanate)iron(II) Complexes via Steric and Noncovalent Interactions. Inorg. Chem 2021, 60, 2045–2055. [PubMed: 33464882]
49. Connelly NG; Geiger WE Chemical Redox Agents for Organometallic Chemistry. Chem. Rev 1996, 96, 877–910. [PubMed: 11848774]
50. Leslie Dutton P., [23] Redox potentiometry: Determination of midpoint potentials of oxidation-reduction components of biological electron-transfer systems. In Meth. Enzymol; Academic Press, 1978; pp 411–435.
51. Nissim R; Compton RG Nonenzymatic Electrochemical Superoxide Sensor. ChemElectroChem 2014, 1, 763–771.
52. Kisaburo U. Electrochemical Studies of the Reduction Mechanism of Tetrazolium Salts and Formazans. Bull. Chem. Soc. Jpn 1989, 62, 3783–3789.
53. Basuli D; Tesfay L; Deng Z; Paul B; Yamamoto Y; Ning G; Xian W; McKeon F; Lynch M; Crum CP; Hegde P; Brewer M; Wang X; Miller LD; Dyment N; Torti FM; Torti SV Iron addiction: a novel therapeutic target in ovarian cancer. Oncogene 2017, 36, 4089–4099. [PubMed: 28319068]
54. Pinnix ZK; Miller LD; Wang W; D'Agostino R; Kute T; Willingham MC; Hatcher H; Tesfay L; Sui G; Di X; Torti SV; Torti FM Ferroportin and Iron Regulation in Breast Cancer Progression and Prognosis. Sci. Transl. Med 2010, 2, 43ra56.

55. Nelson RL Iron and colorectal cancer risk: Human studies. Nutr. Rev 2001, 59, 140–148. [PubMed: 11396694]

56. Bedford MR; Ford SJ; Horniblow RD; Iqbal TH; Tselepis C Iron Chelation in the Treatment of Cancer: A New Role for Deferasirox? J. Clin. Pharmacol 2013, 53, 885–891. [PubMed: 23740857]

57. Lui GYL; Obeidy P; Ford SJ; Tselepis C; Sharp DM; Jansson PJ; Kalinowski DS; Kovacevic Z; Lovejoy DB; Richardson DR The Iron Chelator, Deferasirox, as a Novel Strategy for Cancer Treatment: Oral Activity Against Human Lung Tumor Xenografts and Molecular Mechanism of Action. Mol. Pharmacol. 2013, 83, 179. [PubMed: 23074173]

58. Salehi S; Saljooghi AS; Shiri A Synthesis, characterization and in vitro anticancer evaluations of two novel derivatives of deferasirox iron chelator. Eur. J. Pharmacol 2016, 781, 209–217. [PubMed: 27090924]

59. Yu Y; Kovacevic Z; Richardson DR Tuning Cell Cycle Regulation with an Iron Key. Cell Cycle 2007, 6, 1982–1994. [PubMed: 17721086]

60. Li N; Chen Q; Gu J; Li S; Zhao G; Wang W; Wang Z; Wang X Synergistic inhibitory effects of deferasirox in combination with decitabine on leukemia cell lines SKM-1, THP-1, and K-562. Oncotarget 2017, 8, 36517–36530. [PubMed: 28388554]

61. Harima H; Kaino S; Takami T; Shinoda S; Matsumoto T; Fujisawa K; Yamamoto N; Yamasaki T; Sakaida I Deferasirox, a novel oral iron chelator, shows antiproliferative activity against pancreatic cancer in vitro and in vivo. BMC Cancer 2016, 16, 702. [PubMed: 27582255]

62. Breuer W; Epsztejn S; Cabantchik ZI Iron Acquired from Transferrin by K562 Cells Is Delivered into a Cytoplasmic Pool of Chelatable Iron(II). J. Biol. Chem 1995, 270, 24209–24215. [PubMed: 7592626]

63. Hentze MW; Muckenthaler MU; Galy B; Camaschella C Two to Tango: Regulation of Mammalian Iron Metabolism. Cell 2010, 142, 24–38. [PubMed: 20603012]

64. Zhang Y; Cai X; Wang Y; Zhang C; Li L; Choi S-W; Wang LV; Xia Y Noninvasive Photoacoustic Microscopy of Living Cells in Two and Three Dimensions through Enhancement by a Metabolite Dye. Angew. Chem. Int. Ed 2011, 50, 7359–7363.

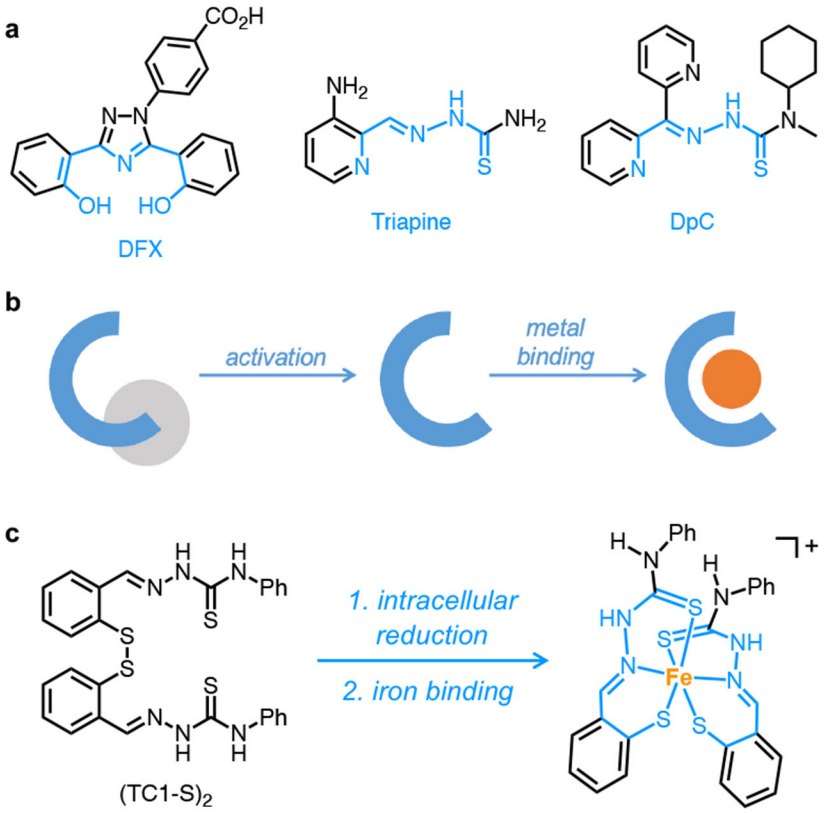


**Figure 1.**

Iron binding in medicine: a) Selected iron chelators evaluated as anticancer agents in clinical trials; b) General prochelation strategy; and c) Example of disulfide-based prochelator activated by intracellular reduction.

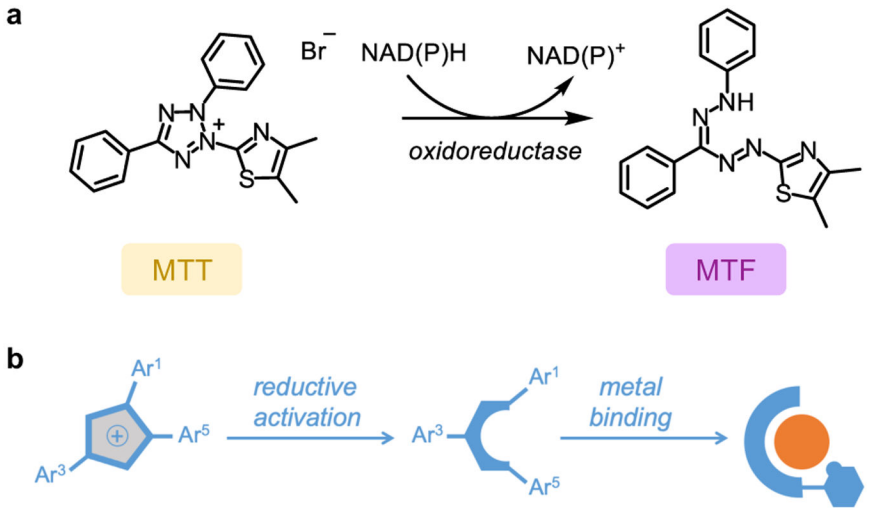


**Figure 2.**

A prochelation strategy inspired by the chemistry of tetrazolium cations: a) Bioreduction of the MTT reagent employed to assess the viability of eukaryotic cells; b) Schematic of the activation of a triaryltetrazolium prochelator to release a formazan ligand carrying a metal-binding donor.

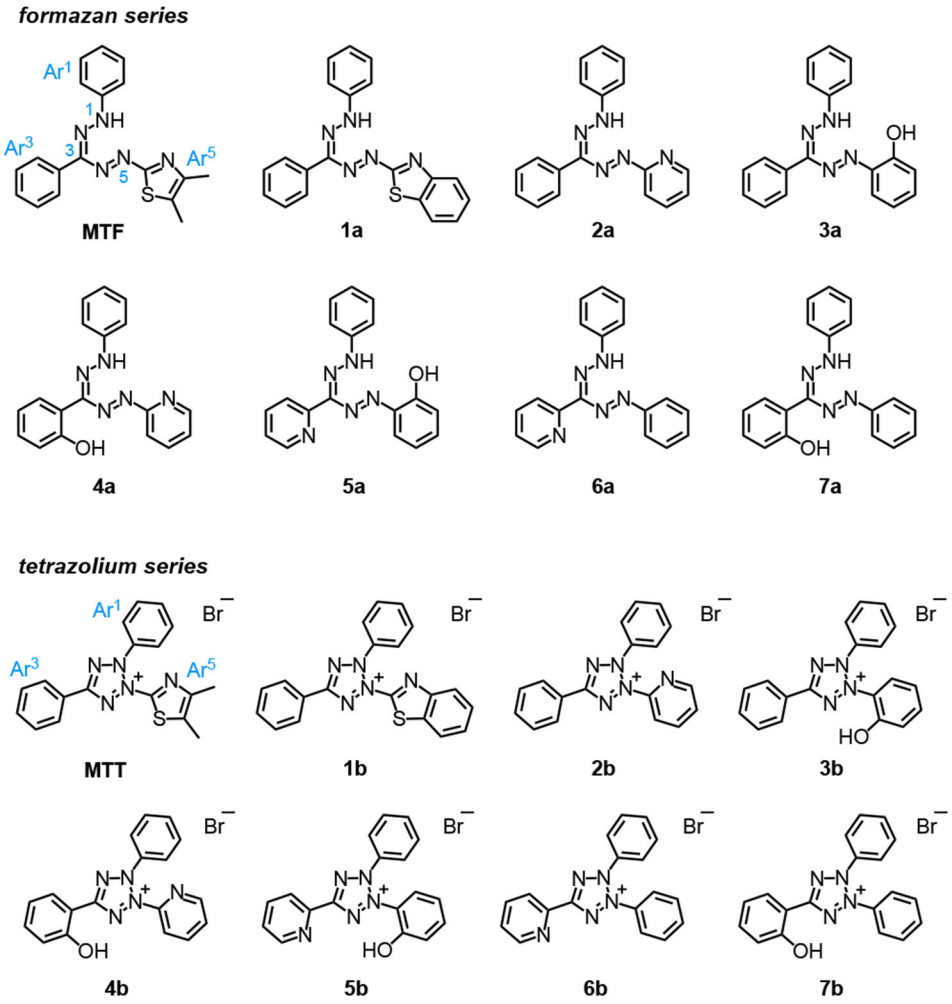


**Figure 3.**
Structures of the formazan and tetrazolium scaffolds investigated in this study.

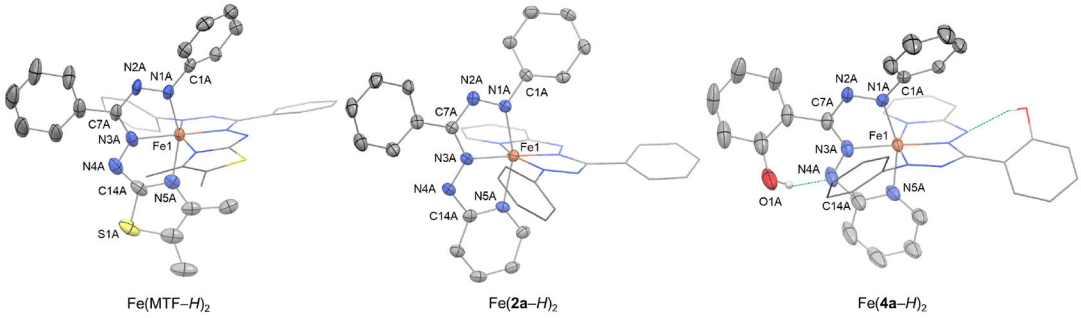


**Figure 4.**

Crystal structures of Fe(MTF–*H*)$_2$, Fe(**2a**–*H*)$_2$, and Fe(**4a**–*H*)$_2$ showing a partial atom labeling scheme. Thermal ellipsoids are scaled to the 50% probability level. In each complex, one of the ligands is shown as capped sticks, and carbon-bound hydrogen atoms are omitted for clarity (CCDC, Fe(MTF–*H*)$_2$ 2217720, Fe(**2a**–*H*)$_2$ 2217721 and Fe(**4a**–*H*)$_2$ 2217722).

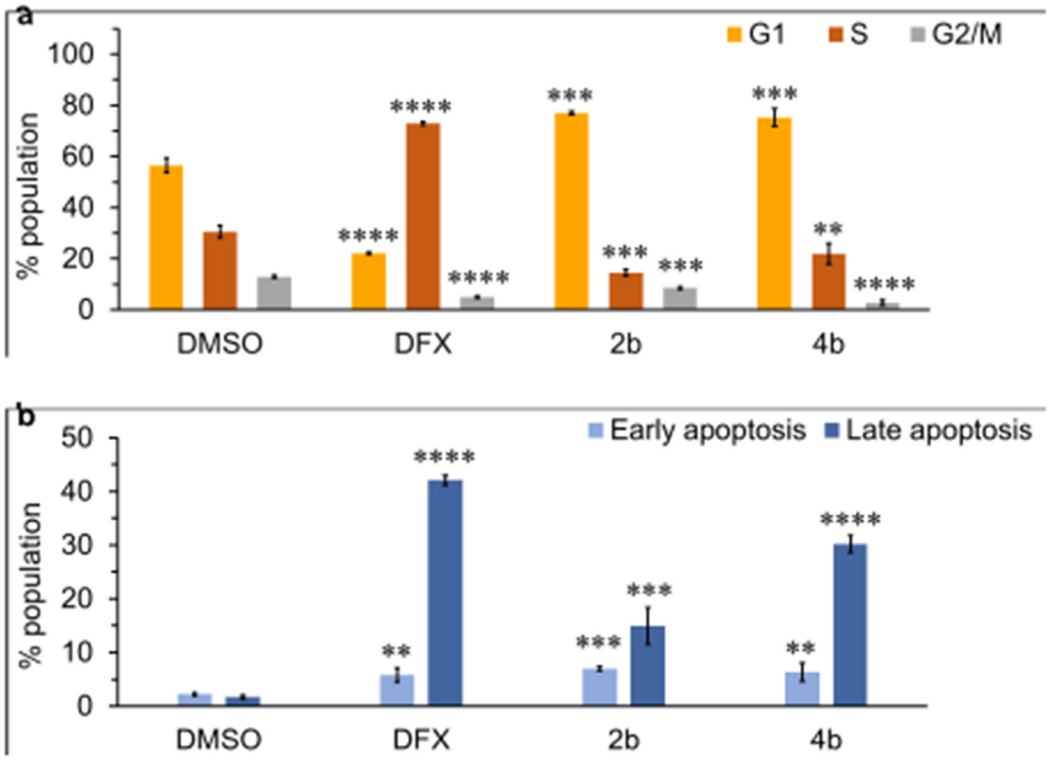


**Figure 5.**

Effects of prochelators **2b** and **4b** on cell cycle and cell death as assessed by flow cytometry in A2780 ovarian cancer cells. (a) Cell cycle distribution after treatment with the test compounds (40 μM) for 24 h; (b) Apoptotic cell death after incubation with the test compounds (40 μM) for 48 h. Experiments were conducted in triplicate and the values shown are mean ± standard deviation. All T-tests relative to vehicle only (DMSO): ** $p < 0.01$, *** $p < 0.001$, **** $p < 0.0001$.

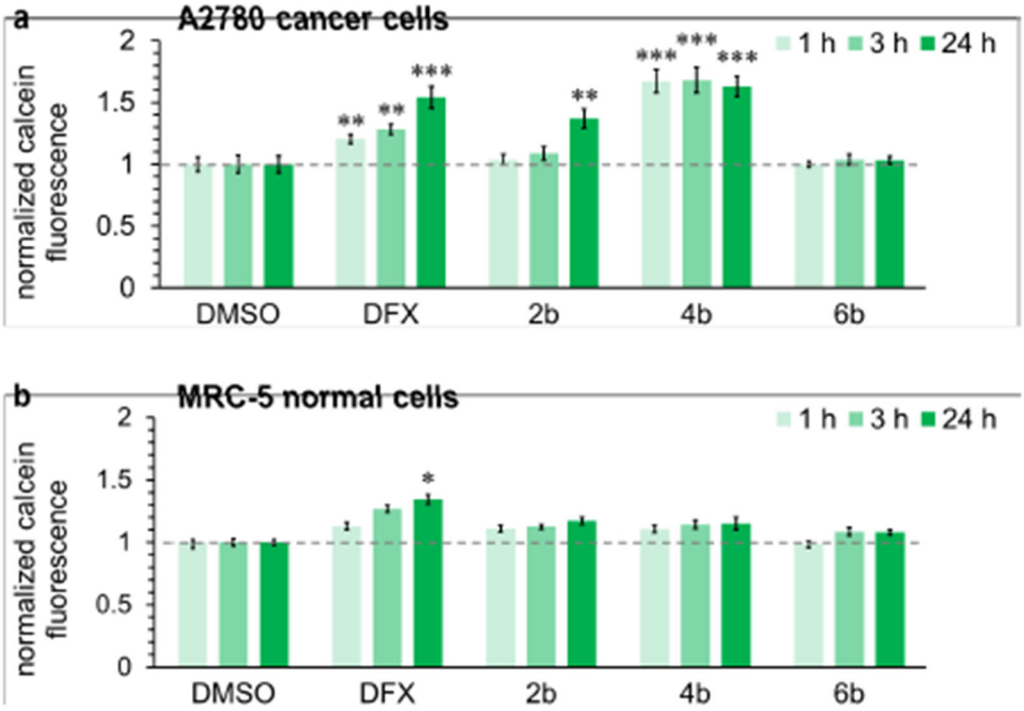


**Figure 6.**

Relative extent of intracellular iron binding assessed through the calcein assay after incubation with the test compounds (40 μM) in A2780 ovarian cancer cells (a) and MRC-5 normal lung fibroblasts (b). Experiments in triplicate shown as mean ± standard deviation. All T-tests relative to vehicle only (DMSO): * $p < 0.05$, ** $p < 0.01$, *** $p < 0.001$.

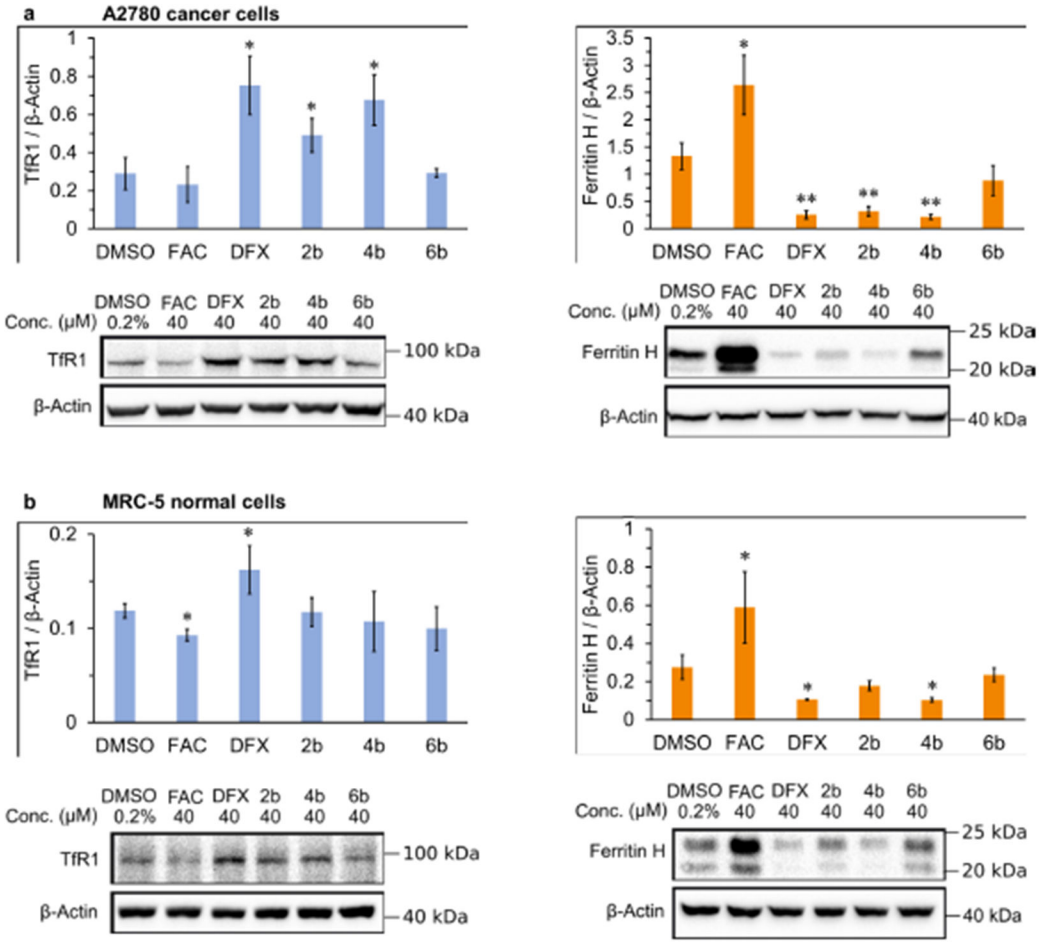


**Figure 7.**

Effects of the prochelators on the expression of transferrin receptor 1 (TfR1) and ferritin heavy chain (ferritin H): Western blot analysis (n=4) and representative gel images after treatment with test compounds for 24 h in A2780 cancer cells (a) and normal MRC-5 cells (b). β-Actin was used as a loading control. All T-tests relative to vehicle only (DMSO): * $p < 0.05$, ** $p < 0.01$.

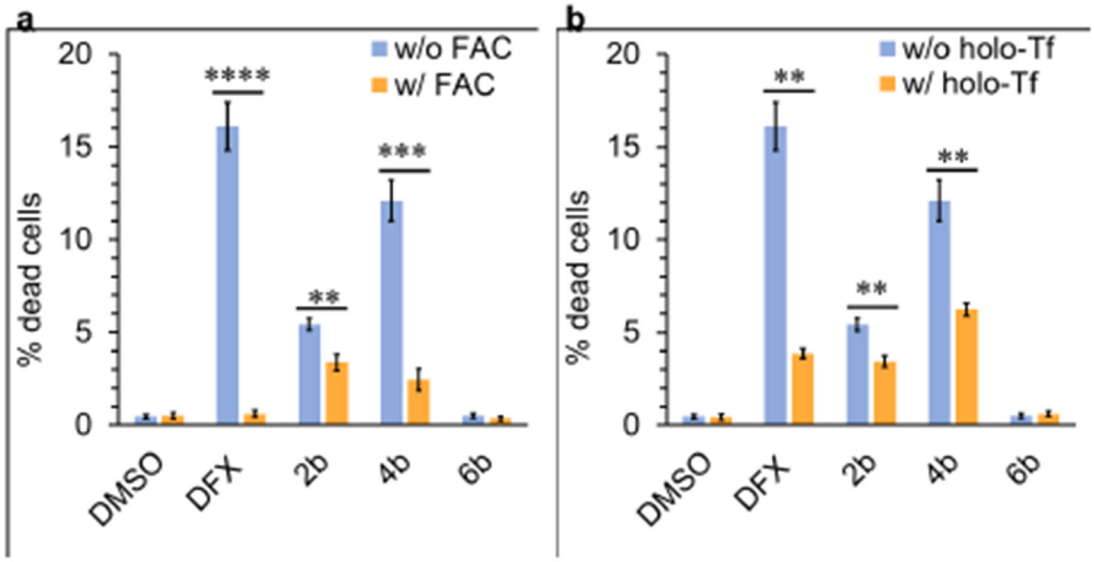


**Figure 8.**

Effects of iron supplementation on toxicity in A2780 cells. The percentage of dead cells was determined using the LIVE/DEAD kit as measured by flow cytometry. Quantification of dead cells after treatment with test compounds (40 μM, 48 h) in the presence or absence of (a) ferric ammonium citrate (FAC, 50 μM) or (b) holo-transferrin (holo-Tf, 50 μM). Experiments in triplicate and values shown as mean ± standard deviation. T-tests relative to sample without iron supplementation: ** $p < 0.01$, *** $p < 0.001$, **** $p < 0.0001$.

**Table 1.**

Log $D_{o/pH7.4}$, reduction potentials, stability in serum, and antiproliferative activities

| | Log $D_{o/pH7.4}$[a] | $E_{red}$[b] (mV vs NHE) | Stability[c] (serum, 24 h) | $IC_{50}$ (μM)[e] | | | | |
|---|---|---|---|---|---|---|---|---|
| | | | | A2780 (Ovary) | MDA-MB-231 (Breast) | Caco-2 (Colon) | A549 (Lung) | MRC-5 (Normal lung) |
| **DFX** | 0.9 | n.d. | n.d. | 15±1 | 17±1 | 67±2 | 21±3 | 220±20 |
| **MTT** | 0.1 | 94 | 58% | 45±9 | 48±7 | 92±7 | 44±9 | 32±5 |
| **1b** | 0.9 | 207 | 2%[d] | 23±3 | 21±2 | 40±3 | 41±3 | 97±10 |
| **2b** | −0.5 | −130 | 100% | 16±3 | 16±2 | 13±2 | 17±2 | 210±20 |
| **3b** | 1.9 | −328 | 100% | 160±20 | 320±20 | 250±80 | 320±20 | 330±40 |
| **4b** | 0.1 | −102 | 100% | 12±3 | 17±2 | 29±3 | 28±4 | 160±20 |
| **5b** | 0.6 | −380 | 100% | 98±10 | 160±20 | 200±50 | 500±80 | >900 |
| **6b** | −1.8 | −241 | 100% | 74±4 | 210±40 | 270±40 | 100±10 | >900 |
| **7b** | −0.1 | −187 | 93% | 74±7 | 130±30 | 280±60 | 180±20 | >900 |

[a] Distribution coefficients log $D_{o/pH7.4}$ values determined by HPLC using the shake-flask method in octanol and PBS (pH 7.4).

[b] Reduction potentials $E_{red}$ measured by cyclic voltammograms (100 mV $s^{-1}$) at a glassy carbon working electrode using potassium ferricyanide ($K_3[Fe(CN)_6]$) as a reference ($E_0$ = 0.430 V vs NHE, 25 °C).[50]

[c] Stability in fetal bovine serum monitored by HPLC for 24 h.

[d] Half-life $t_{1/2}$ = 2 h.

[e] $IC_{50}$ values (mean ± SDM, n=3) obtained using the resazurin assay after exposure to test compounds (0.16–100 μM or 11–900 μM) for 72 h.